Chemistry of Metals and Alloys

Chem. Met. Alloys 17 (2024) 53-57
Ivan Franko National University of Lviv
http://publications.lnu.edu.ua/chemetal

Phase equilibria in the Er–Zr–Sb ternary system at 1073 K

L. ROMAKA[1]*, Yu. STADNYK[1], A. ZELINSKII[1]

[1] *Department of Inorganic Chemistry, Ivan Franko National University of Lviv, Kyryla i Mefodiya St. 6, 79005 Lviv, Ukraine*
* *Corresponding author. E-mail: lyubov.romaka@lnu.edu.ua*

Received October 11, 2024; accepted December 17, 2024
https://doi.org/10.30970/cma17.0448

The phase equilibrium diagram of the ternary system Er–Zr–Sb was constructed in the full concentration range at 1073 K, using X-ray powder diffraction, microstructural analyzis, and energy-dispersive X-ray spectroscopy. At the temperature of investigation, the Er–Zr–Sb system is characterized by the formation of one ternary compound, ErZrSb (structure type UGeTe, space group *I*4/*mmm*, *a* = 0.4217(3), *c* = 1.6165(4) nm). A significant homogeneity range was established along the isoconcentrate 33.3 at.% Sb, extending from 25 to 33 at.% Er. The solubility of Zr in the binary compounds ErSb and Er_5Sb_3 extends to ~2 and ~3 at.%, respectively.

Intermetallics / Phase diagram / X-ray diffraction / Scanning electron microscopy

1. Introduction

Experimental studies of the interaction between the components in metallic systems is an important stage to obtain information regarding peculiarities of the formation, stability with respect to temperature and concentration, and crystal structure of intermediate phases for further study of the physical properties of intermetallics. *R*–Zr–Sb ternary systems (*R* = rare-earth metal) have been studied over the whole concentration range for *R* = Ce (873 K) [1], Sm (1070 K) [2], Gd (873 K) [1], and Dy (1070 K) [3]. In the Sm–Zr–Sb system no ternary compounds were detected at 1070 K. However, in [4] the ternary compounds R_3ZrSb_5 (*R* = La, Ce, Pr, Nd, Sm) with Hf_5CuSn_3 structure type were reported. According to literature data, in the *R*–Zr–Sb systems where *R* is a rare earth of the Y subgroup, equiatomic *R*ZrSb compounds with UGeTe-type structure (superstructure of the La_2Sb-type, space group *I*4/*mmm*) are formed [5]. New representatives of the structure type UGeTe were found for $R_xZr_{2-x}Sb$ ($x \approx 0.1$) with *R* = La-Nd, Sm at 873 K [6]. For GdZrSb and DyZrSb a large homogeneity range along the isoconcentrate 33.3 at.% Sb was established [1,3]. Some *R*ZrSb antimonides exhibit interesting magnetic behavior. Magnetic measurements showed magnetic ordering at low temperature and strong coercive fields for TbZrSb and DyZrSb [7]. The ErZrSb compound is characterized by an incommensurate magnetic structure [8].

In this contribution we report experimental results of an investigation of the isothermal section at 1073 K of the phase diagram of the Er–Zr–Sb ternary system in the full concentration range.

2. Experimental

To construct the phase equilibrium diagram of the Er–Zr–Sb ternary system, polycrystalline samples were synthesized by direct arc-melting of the constituent metals (erbium, purity 99.9 wt.%; zirconium, purity 99.99 wt.%; antimony, purity 99.999 wt.%.) in a protected argon atmosphere with a non-consumable tungsten electrode, on a water-cooled copper hearth. To remove traces of impurities, first a Ti ingot was melted as a getter. To compensate for the evaporative losses of antimony during arc-melting, 2-3 wt.% excess Sb, depending on the sample composition, was added. For better homogenization the alloys were re-melted twice. After melting, the overall weight losses of the alloys were generally less than 1 wt.%. Pieces of the arc-melted ingots were then placed in evacuated quartz ampoules and annealed at 1073 K for 700 h. The annealed ingots were removed from the furnace and quenched in cold water.

Powder X-ray diffraction (XRPD) was used for the construction of the phase diagram (determination of the phase fields, identification of intermediate phases, formation of solid solutions). The observed diffraction

intensities of the powder patterns (DRON-2.0, Fe *K*α radiation) were compared with reference powder patterns of the constituent elements and known binary and ternary phases (program PowderCell [9]). Elemental and phase compositions of the prepared samples were examined by scanning electron microscopy (SEM) using a Tescan Vega 3 LMU scanning microscope with a Link EDX system operated at 20 kV and 60 μA. Quantitative electron probe microanalysis (EPMA) of the phases was carried out using an energy-dispersive X-ray analyzer with the pure elements as standards (typical acceleration voltage was 20 kV; *K*- and *L*-lines were used). For each phase, 3-5 measurements were made to obtain an average value.

Calculations of the crystallographic parameters were performed using the WinCSD [10] program package.

3. Results and discussion

3.1. Binary boundary systems

The binary boundary systems that delimit the ternary Er–Zr–Sb system have been investigated previously; the binary compounds are briefly described below.

Zr–Sb. The version of the phase diagram accepted here is taken from [11,12]. Under the conditions used here, five binary compounds form in this system, Zr_3Sb (Ni_3P structure type), Zr_2Sb (La_2Sb structure type), Zr_5Sb_3 (Mn_5Si_3 structure type), ZrSb (ZrSb structure type), and $ZrSb_2$ ($TiAs_2$ structure type).

Er–Sb. The Er–Sb phase diagram was reported in [13]. Three compounds were found: Er_5Sb_3, ErSb, and $ErSb_2$. ErSb melts congruently, Er_5Sb_3 and $ErSb_2$ are formed by peritectic reactions. Two polymorphic forms of Er_5Sb_3 were studied in [14]. It was found that the low-temperature form belongs to the hexagonal Mn_5Si_3-type, while the high-temperature modification crystallizes in the orthorhombic β-Yb_5Sb_3 structure type. Er_3Sb_4 with Th_3P_4-type structure was reported in [15].

Er–Zr. The phase diagram as assessed in the compilation [16] was used for our investigation. No binary compounds are formed. The solubility of Zr in Er extends up to 20 at.% at 1573 K and decreases with decreasing temperature down to 12.5 at.%. The solubility of Er in Zr extends up to ~3 at.%.

Crystallographic characteristics of the binary compounds in the Er–Sb and Zr–Sb systems at 1073 K are gathered in Table 1.

3.2. Isothermal section of the Er–Zr–Sb system

To construct the phase equilibrium diagram of the Er–Zr–Sb ternary system, 25 ternary and binary alloys were synthesized, annealed at 1073 K and examined by XRPD and EPMA. Based on the results of the analyses, the isothermal section of the phase diagram of the Er–Zr–Sb system was constructed over the whole concentration range at 1073 K (Fig. 1). As regards to the boundary systems, the presence of almost all binary compounds in the Er–Sb and Zr–Sb systems reported in the literature was confirmed at 1073 K (Table 1, Fig. 1). At the temperature of investigation, 1073 K, Er_5Sb_3 crystallizes with the orthorhombic Yb_5Sb_3 structure type (Table 1). During a previous study of the Er–Ni–Sb ternary system [17] the Er_5Sb_3 binary was examined both in as-cast state and after annealing at 1073 K. Phase analysis of the annealed Er_5Sb_3 sample clearly showed the presence of the orthorhombic modification with Yb_5Sb_3-type structure (a = 1.1698, b = 0.9128, c = 0.8022 nm).

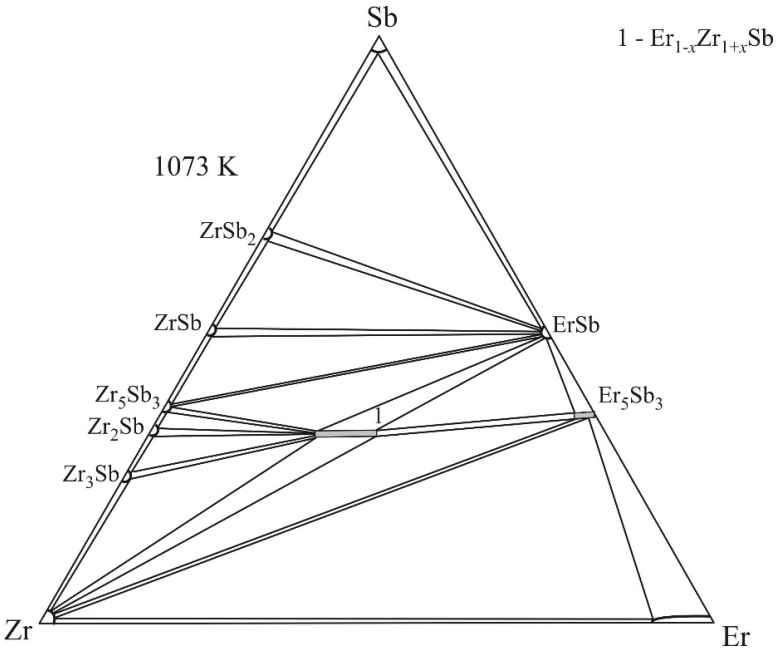

Fig. 1 Isothermal section of the phase diagram of the Er–Zr–Sb system at 1073 K.

Table 1 Binary phases relevant to the 1073 K isothermal section of the Er–Zr–Sb system (p – peritectic reaction; m – congruent melting).

Phase	Melting temperature, K	Pearson symbol, structure type	Lattice parameters, nm			Reference
			a	*b*	*c*	
ErSb	m 2313	*cF*8, NaCl	0.6117(3)	–	–	This work
Er_5Sb_3	p 1913	*oP*32, Yb_5Sb_3	1.1698	0.9128	0.8022	[17]
$ZrSb_2$	?	*oP*24, $TiAs_2$	0.9948	1.4932	0.3875	[2]
ZrSb	?	*oS*24, ZrSb	0.3827	1.0426	1.4007	[12]
Zr_5Sb_3	m 2173	*hP*16, Mn_5Si_3	0.8477(3)	–	0.5817(3)	This work
Zr_2Sb	p 1933	*tI*12, La_2Sb	0.41172	–	1.5771	[12]
Zr_3Sb	?	*tI*32, Ni_3P	1.1335(2)	–	0.5683(4)	This work

Table 2 Composition of selected alloys in the Er–Ni–Sb system from EPMA data.

Phase	Structure type	Er, at.%	Zr, at.%	Sb, at.%
$Er_{55}Zr_{20}Sb_{25}$ ($Er_{53.73}Zr_{22.69}Sb_{23.58}$)				
Er_5Sb_3	Yb_5Sb_3	61.67	1.87	36.46
(Er,Zr)	Mg	86.33	13.67	-
$Er_{35}Zr_{40}Sb_{25}$ ($Er_{34.73}Zr_{41.34}Sb_{23.93}$)				
ErZrSb	UGeTe	33.45	32.51	34.04
Er_5Sb_3	Yb_5Sb_3	59.88	3.08	37.04
Zr	Mg	2.18	97.82	-
$Er_{35}Zr_{25}Sb_{40}$ ($Er_{34.87}Zr_{24.45}Sb_{40.68}$)				
ErZrSb	UGeTe	25.35	41.19	33.46
ErSb	NaCl	48.19	1.58	50.23
Zr_5Sb_3	Mn_5Si_3	61.88	1.35	36.77
$Er_{40}Zr_{30}Sb_{30}$ ($Er_{41.83}Zr_{26.45}Sb_{31.72}$)				
ErZrSb	UGeTe	33.42	32.71	33.87
Er_5Sb_3	Yb_5Sb_3	60.71	2.63	36.66
Zr	Mg	98.17	1.83	-
$Er_{15}Zr_{40}Sb_{45}$ ($Er_{14.89}Zr_{40.29}Sb_{44.82}$)				
ErSb	NaCl	48.21	1.65	50.14
ZrSb	ZrSb	1.07	49.49	49.44
Zr_5Sb_3	Mn_5Si_3	62.47	1.17	36.36
$Er_{50}Zr_{20}Sb_{30}$ ($Er_{48.89}Zr_{22.25}Sb_{28.86}$)				
ErZrSb	UGeTe	33.82	32.37	33.81
Er_5Sb_3	Yb_5Sb_3	61.13	2.24	36.63
Zr	Mg	96.88	3.12	-
$Er_{20}Zr_{25}Sb_{55}$ ($Er_{19.79}Zr_{25.43}Sb_{54.78}$)				
$ZrSb_2$	$TiAs_2$	0.91	32.18	66.91
ZrSb	ZrSb	1.12	49.51	49.37
ErSb	NaCl	48.17	1.72	50.11
$Er_{45}Zr_{15}Sb_{40}$ ($Er_{44.82}Zr_{15.43}Sb_{39.75}$)				
ErZrSb	UGeTe	33.49	32.84	33.67
ErSb	NaCl	48.27	1.61	50.12
Er_5Sb_3	Yb_5Sb_3	62.13	1.24	36.63

As shown in Fig. 1, the isothermal section of the phase diagram of the Er–Zr–Sb system at 1073 K in the full concentration range consists of 10 three-phase, 20 two-phase and 11 single-phase regions. The highest number of solid-state equilibria are formed by the ErZrSb ternary antimonide. Phase compositions of some of the alloys from EPMA data are presented in Table 2. Microphotographs of selected alloys are presented in Fig. 2.

At the temperature of investigation, 1073 K, the existence of the ternary compound ErZrSb with UGeTe structure type (space group *I*4/*mmm*) [5] was confirmed in the Er–Zr–Sb system. For the ErZrSb compound, similarly to the previously studied compounds GdZrSb and DyZrSb [1,3], a homogeneity range along the isoconcentrate 33.3 at.% Sb in the direction toward higher zirconium content was found (Fig. 1). According to the results of the EPM analysis,

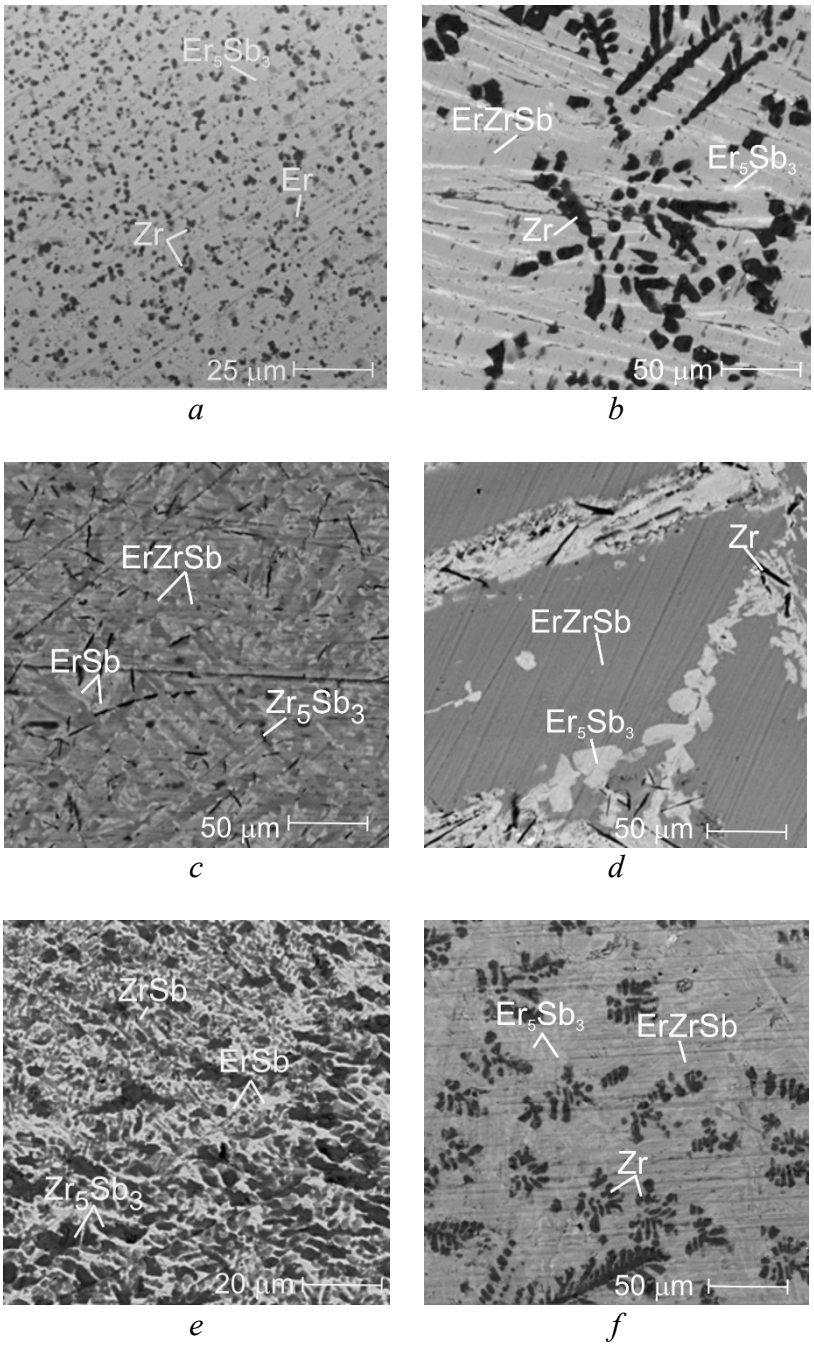

Fig. 2 SEM pictures of alloys from the Er–Zr–Sb system: *a*) $Er_{55}Zr_{20}Sb_{25}$; *b*) $Er_{35}Zr_{40}Sb_{25}$; *c*) $Er_{35}Zr_{25}Sb_{40}$; *d*) $Er_{40}Zr_{30}Sb_{30}$; *e*) $Er_{15}Zr_{40}Sb_{45}$; *f*) $Er_{50}Zr_{20}Sb_{30}$.

the homogeneity range is limited by the compositions $Er_{32.89}Zr_{33.08}Sb_{34.03}$ and $Er_{24.44}Zr_{42.37}Sb_{33.19}$ ($Er_{1-0.75}Zr_{1-1.25}Sb$, a = 0.4217(2)-0.4203(3), c = 1.6165(4)-1.6148(5) nm).

The solubility of Er in the binary compounds of the Zr–Sb system under the conditions used here is insignificant (up to 1.5 at.%). In order to determine the solubility of Zr in ErSb, similarly as done for the Er–Ni–Sb ternary system, several alloys along the lines ErZrSb–ErSb and ErSb–ZrSb were prepared and examined. It was found that the ErSb binary compound (NaCl structure type) dissolves up to ~2 at.% Zr along the isoconcentrate 50 at.% Sb. According to the EPMA data, the limit of solubility corresponds to the composition $Er_{48.92}Zr_{1.68}Sb_{49.40}$. Er_5Sb_3 dissolves up to 3 at.% Zr along the isoconcentrate 37.5 at.% Sb. EPMA data of the $Er_{35}Zr_{40}Sb_{25}$ sample (Fig. 2b) shows the $Er_{5-x}Zr_xSb_3$ phase ($Er_{59.88}Zr_{3.08}Sb_{37.04}$) in equilibrium with ErZrSb and Zr.

Comparing the Er–Zr–Sb system investigated in our work and the {Gd,Dy}–Zr–Sb systems studied earlier [1,3], we may note that the low number of ternary phases in the Er–Zr–Sb systems does not differ from

the reported Gd–Zr–Sb and Dy–Zr–Sb systems. In all these systems equiatomic *R*ZrSb compounds, characterized by a significant homogeneity range from the stoichiometric composition to a composition with lower rare-earth content, are present. A comparison of the Er–Zr–Sb system and the Er–Ti–Sb [18], Er–Fe–Sb [19], and Er–Ni–Sb [17] systems showed the influence of the nature of the *d*-element on the interaction between the components. No ternary compounds were found in the Er–Ti–Sb system, whereas in the Er–Fe–Sb system one ternary antimonide, Er_6FeSb_2 with K_2UF_6-type structure, was observed. Both the Er–Zr–Sb and Er–Ni–Sb systems are characterized by the presence of equiatomic compounds, but with different structure types. The half-Heusler intermetallic compound ErNiSb belongs to the cubic structure type MgAgAs [20], while ErZrSb crystallizes with the tetragonal UGeTe-type.

Conclusion

The phase equilibrium diagram of the Er–Zr–Sb system was constructed at 1073 K over the whole concentration range based on X-ray powder diffraction and energy-dispersive X-ray spectroscopy. It was established that at the temperature of investigation the Er–Zr–Sb system is characterized by the existence of one ternary compound, ErZrSb with UGeTe-type structure. The solubility limit of Zr in the ErSb and Er_5Sb_3 binaries was found to be ~2 and 3 at.%, respectively. The homogeneity range of the ErZrSb antimonide was established; it extends from 25 to 33 at.% Er along the isoconcentrate 33.3 at.% Sb.

Acknowledgements

The work was carried out within the framework of the Ministry of Education of Ukraine (grant No. 0124U000989). The authors also thank the Simons Foundation (SFI-PD-Ukraine-00014574) for support.

References

[1] O. Senchuk, R.E. Gladyshevskii, *Solid State Phenom.* 289 (2019) 3-12. https://doi.org/10.4028/www.scientific.net/SSP.289.3

[2] A.V. Morozkin, *J. Alloys Compd.* 336 (2002) 187-189. https://doi.org/10.1016/S0925-8388(01)01882-5

[3] A.V. Morozkin, I.A. Sviridov, A.V. Leonov, *J. Alloys Compd.* 335 (2002) 139-141. https://doi.org/10.1016/S0925-8388(01)01814-X

[4] G. Bollore, M.J. Ferguson, R.W. Hushagen, A. Mar, *Chem. Mater.* 7 (1995) 2229-2231. https://doi.org/10.1021/cm00060a005

[5] A.V. Morozkin, I.A. Sviridov, *J. Alloys Compd.* 320 (2001) L1-L2. https://doi.org/10.1016/S0925-8388(01)00943-4

[6] O. Senchuk, Ya. Tokaychuk, R. Gladyshevskii, *Chem. Met. Alloys* 16 (2023) 22-25. https://doi.org/10.30970/cma16.0435

[7] R. Welter, A.V. Morozkin, K. Halich, *J. Magn. Magn. Mater.* 257 (2003) 44-50. https://doi.org/10.1016/S0304-8853(02)00984-8

[8] A.V. Morozkin, K. Halich, R. Welter, B. Ouladdiaf, *J. Alloys Compd.* 393 (2005) 34-40. https://doi.org/10.1016/j.jallcom.2004.09.051

[9] W. Kraus, G. Nolze, *J. Appl. Crystallogr.* 29 (1996) 301-303. https://doi.org/10.1107/S0021889895014920.

[10] L. Akselrud, Yu. Grin, *J. Appl. Crystallogr*. 47 (2014) 803-805. https://doi.org/10.1107/S1600576714001058

[11] T.B. Massalski, Binary Alloys Phase Diagrams, ASM International, Metals Park, Ohio, 1990.

[12] E. Garcia, J.D. Corbett, *J. Solid State Chem*. 73 (1988) 452-467. https://doi.org/10.1016/0022-4596(88)90131-4

[13] M.N. Abdusalyamova, O.I. Rachmatov, *J. Alloys Compd*. 299 (2000) L1-L3. https://doi.org/10.1016/S0925-8388(99)00581-2

[14] M. Zelinska, O. Zhak, S. Oryshchyn, V. Babizhetskyy, J.-I. Pivan, R. Guérin, *J. Alloys Compd.* 437 (2007) 133-139. https://doi.org/10.1016/j.jallcom.2006.07.087

[15] M.N. Abdusalyamova, N.A. Vlasov, Y.M. Goryachev, *Inorg. Mater*. 20 (1984) 1242-1245.

[16] H. Okamoto, *Phase Diagrams for Binary Alloys,* Materials Park (OH): ASM, 2000.

[17] L. Romaka, Yu. Stadnyk, P. Klyzub, *Chem. Met. Alloys* 17 (2024) 5-12. https://doi.org/10.30970/cma17.0439

[18] H. Bie, S.H. Devon Moore, D.G. Piercey, A.V. Tkachuk, O.Ya. Zelinska, A. Mar, *J. Solid State Chem*. 180 (2007) 2216-2224. https://doi.org/10.1016/j.jssc.2007.05.030

[19] G. Cai, X. Wei, L. Zeng, *J. Alloys Compd.* 420 (2006) 133-135. https://doi.org/10.1016/j.jallcom.2005.10.039

[20] K. Hartjes, W. Jeitschko, *J. Alloys Compd.* 226 (1995) 81-86. https://doi.org/10.1016/0925-8388(95)01573-6